Proc. Indian Acad. Sci. (*Chem. Sci.*), Vol. 115, Nos 5 & 6, October–December 2003, pp 533–542

Electrostatic potential profile and nonlinear current in an interacting one-dimensional molecular wire¶

S LAKSHMI and SWAPAN K PATI*
Theoretical Sciences Unit, Jawharlal Nehru Centre for Advanced Scientific Research, Jakkur Campus, Bangalore 560 064, India
e-mail: pati@jncasr.ac.in

Abstract. We consider an interacting one-dimensional molecular wire attached to two metal electrodes on either side of it. The electrostatic potential profile across the wire-electrode interface has been deduced solving the Schrodinger and Poisson equations self-consistently. Since the Poisson distribution crucially depends on charge densities, we have considered different Hamiltonian parameters to model the nano-scale wire. We find that for very weak electron correlations, the potential gradient is almost zero in the middle of the wire but are large near the chain ends. However, for strong correlations, the potential is essentially a ramp function. The nonlinear current, obtained from the scattering formalism, is found to be less with the ramp potential than for weak correlations. Some of the interesting features in current–voltage characteristics have been explained using one-electron formalism and instabilities in the system.

Keywords. Molecular wire; extended Hubbard model; potential profile, nonlinear current; chemisorption.

1. Introduction

The term molecular wire refers to a molecule between two macroscopic electrodes which act as continuum reservoirs of electrons. A molecule refers to a quantum dot, several orders of magnitude smaller than the usual semiconducting quantum dot. What happens when such a small quantum dot is connected between two macroscopic electrodes has been the subject of interest over the last few years.[1–3] Experimentally, several groups have reported transport measurements on a single or a small group of molecules.[4–8] These developments have attracted much attention since these are very important systems from a semiconductor industry point of view. Furthermore, it is important from the point of view of basic physics since it offers a challenging opportunity to understand the effects of many-body interactions on their capabilities to serve as active components in molecular electronics.[9]

With the advent of a number of new experimental techniques, the field has grown enormously over the last few years.[10] Theoretically too, the calculations have been performed on a large number of systems using semi-empirical to first-principles methods.[11–13] These studies have been mainly focussed on the mechanisms by which these molecular wires conduct, how they operate under the influence of an external driving potential and the recognition of the basic principles for achieving conductance control. It is quite well

¶Dedicated to Professor C N R Rao on his 70th birthday
*For correspondence

known by now that the current in these systems is a nonlinear function of the voltage and depends crucially on the electronic structure of the electrodes as well as of the wire. The transport has been based on Landauer's formalism,[14] which describes the current as the probability that an electron which is initially at the left electrode will be found at the right electrode after ∞ time. Strictly speaking, this formalism holds for elastic scattering which can be assumed by neglecting electron–electron and electron-phonon scatterings.

In this article, we go beyond the noninteracting Hamiltonian, and include explicit electron–electron interactions in the form of extended Hubbard model in the mean field. We have carried out our calculations in an explicit spin basis and have studied the spatial variation of the electrostatic potential across the wire in great detail. We also have computed the nonlinear current through the wire, for varying molecular Hamiltonain parameters. In the next section, we discuss the molecular Hamiltonian and the methods to calculate the nonlinear current. We then discuss the results for a large number of parameters of the Hamiltonain in §3. We end the paper with a summary of all the results.

2. Nonlinear current and the molecular Hamiltonian

Our nanoscale device consists of two metal electrodes and a molecular chain attached between them. The molecule is considered to be a one-dimensional chain of N atoms with one orbital per atomic site. We assume that the electron transfer occurs sufficiently faster than the underlying nuclear motion and hence neglect electron-phonon coupling effects. The coupling between the molecular wire sites and the electrode is considered according to the Newns–Anderson model.[15] We also use the form for the nonlinear current that has been obtained[16] as:

$$J(W) = \frac{2e}{p\hbar} \int_{E_f - eW}^{E_f} \mathrm{d}E \Delta_L(E) \Delta_R(E + eW) \, |G_{1N}(E, W)|^2, \tag{1}$$

where W is the applied voltage, E is the electron-injection energy and $G_{1N}(E, W)$ is the voltage-dependent Green's function matrix element taken between the first and the Nth site of the wire. Δ_L and Δ_R refer to the spectral densities of the left and right electrodes, which is defined according to the Newns–Anderson model[15] as

$$\begin{aligned} \Delta_i(E) &= (b_i^2/g)[1 - (E/2g)^2]^{1/2}, \quad E < 2g \\ &= 0, \quad \text{otherwise} \end{aligned} \tag{2}$$

where $2g$ is the bandwidth of the continuum of the metal electrodes and b_i corresponds to the strength of the chemisorption between the wire and the ith electrode.

The Hamiltonian for the wire needs to be corrected to include the wire-electrode interactions.[17] We assume that the 1st and the last sites of the one-dimensional wire are connected to the left and right electrodes respectively. Thus,

$$\overline{H}_{ii} = H_{ii} - \Sigma_i(E), \quad i = 1 \text{ or } N, \tag{3}$$

where $\Sigma_i(E)$ is the self-energy contribution of the ith reservoir given by,

$$\Sigma_i(E) = \Lambda_i(E) - i\Delta_i(E), \tag{4}$$

where $\Lambda_i(E)$ in the Newns model has the form,

$$\begin{aligned}\Lambda_i(E) &= (b_i^2/g)(E/2g);\ |E/2g|<1\\ &= (b_i^2/g)[(E/2g)+\{(E/2g)^2-1\}^{1/2}];\ (E/2g)<-1\\ &= (b_i^2/g)[(E/2g)-\{(E/2g)^2-1\}^{1/2}];\ (E/2g)>1.\end{aligned} \tag{5}$$

Most of the experimental studies consider organic molecules which are either semiconducting or insulating. Moreover, organic conjugated molecules consisting of carbon atoms have delocalised p-electrons, with strong electron correlations. Noninteracting models cannot even account for its energetics in a qualitative scale. For a serious study, one requires long range Coulomb interactions to describe such systems. However, it has been shown rigorously that the extended Hubbard model with nearest neighbour Coulomb interactions give a very good estimate of their optical as well as transport properties.[18] It is interesting to note that this is the minimal model to account for the excitons in organic systems. The Hamiltonian in explicit form can be written as

$$H = \sum_i \sum_s -t(a_{is}^\dagger a_{i+1s} + hc) + U\sum_i n_{i\uparrow}n_{i\uparrow} + \sum_{ij} V_{ij} n_i n_j, \tag{6}$$

where t is the electron hopping term and U is the Hubbard on-site term. The last term V_{ij} is the electron–electron coulombic repulsion between electrons in adjacent sites.

Since we are using Landauer formula for computing the transport properties, we solve the above Hamiltonian in the mean-field limit. The averaged (mean-field) form of the Hamiltonian can be derived as

$$\begin{aligned}H_{mf} &= -t\sum_i (a_{is}^\dagger a_{i+1s} + hc) + U\sum_{is} a_{i-s}^\dagger a_{i-s} \langle a_{is}^\dagger a_{is}\rangle\\ &\quad -U\sum_i (\langle a_{is}^\dagger a_{i-s}\rangle a_{i\uparrow}^\dagger a_{i\downarrow} + hc) + V\sum_{ijs} \langle a_{is}^\dagger a_{is} + a_{i-s}^\dagger a_{i-s}\rangle n_{js}\\ &\quad -V\sum_{ijss'} (\langle a_{is}^\dagger, a_{is}\rangle a_{is}^\dagger a_{js'} + hc).\end{aligned} \tag{7}$$

Note that the above Hamiltonian is the unrestricted Hartree–Fock equation wherein the spins of the electrons have been treated explicitly.[19] The on-site electron repulsion term for the spin-up electrons is due to the field created by the down-spin electrons. Also as can be seen, the last term in the above equation is an effective hopping term with conservation ($s = s'$) and breaking ($s \neq s'$) of spin symmetry. Thus in the mean-field limit, the V term effectively renormalizes the hopping strength in the system. In our calculations, we start with the tight-binding basis and calculate the mean-quantities in that basis. Then inserting the mean-quantities, we solve the above mean-field Hamiltonian. We then recalculate the mean-quantities in this new basis. This procedure continues until all of the mean-quantities converge. Note that the Hamiltonian is a $2N \times 2N$ dimensional matrix.

In most of the earlier calculations in this field, the electrostatic potential profile due to the applied bias has been assumed to be a ramp function. However, any residual charge in

the molecule would result in polarisation of the metal electrodes due to the image potential. Datta *et al*[20] and later Mujica *et al*[21] have proposed a self-consistent solution of the Poisson equation coupled with the Schrodinger equation to overcome this problem. Indeed, they have suggested that this self-consistent solution is essential to account for the actual features of the current spectra of these nanowires. Mujica *et al* have solved this problem by self-consistently evaluating the charge densities from the Schrödinger equations and then using those as inputs to the Poisson equations.[21] To overcome the boundary conditions on the electrostatic potential profile, they have considered finite but large dielectric constants for the metal electrodes compared to the molecular sites.

We adopt here a similar approach, but the boundary conditions have been properly considered so that the final electrostatic potential field extending from one metal to the other becomes different for different atomic sites. This is to say that when an electric field is applied, the atomic electron density will adjust to the field in such a way that the charges are stabilised locally. We start our self-consistent solution by assuming that the electrostatic field is a linear ramp function across the metal-molecule interface. By solving the above mean-field Hamiltonian as mentioned before, we obtain charge density ($\boldsymbol{r}_i$) at every site, i.

$$r_i = \sum_s a_{is}^{\dagger} a_{is} . \tag{8}$$

This becomes the input in the one-dimensional Poisson equation,

$$W_{i+1} + W_{i-1} - 2W_i = -\boldsymbol{r}_i, \tag{9}$$

where we have assumed that the inter-atomic distance and the dielectric constant at every atomic site are constant and unity. The diagonal elements of the Hamiltonian is then modified as $\tilde{H}_{ii} = H_{ii} - eW_i$. To maintain the boundary conditions, we enforce that the left electrode (to which the atomic site '1' is weakly coupled) has zero bias while the right electrode has the full bias (i.e. W). This ensures that the electrodes are not polarised due to the charge accumulations at the molecular sites. We then obtain the charge densities by solving the modified Hamiltonian and use them in the Poisson equations. This is continued until all the charge densities and all the site potential fields converge. The converged Hamiltonian matrix is then used to compute the Green's function and subsequently the nonlinear current.

3. Results and discussion

The Fermi energies of the metal electrodes are equal and taken to be at the middle of the HOMO–LUMO gap of the energies obtained from the molecular Hamiltonian alone at the zero bias condition. As the bias is turned on, right electrode's Fermi energy is floated by an amount equal to the magnitude of the applied bias, while the left electrode's Fermi energy is kept fixed. We then calculate the Greens function matrix for a given bias. This matrix is also $2N \times 2N$. To calculate current, we require four elements of the this Greens function, two corresponding to the first atomic site and two corresponding to the Nth atomic site. We have done these calculations for a wire of length 20 atomic sites unless otherwise stated and by varying the parameters U and V in the above Hamiltonian.

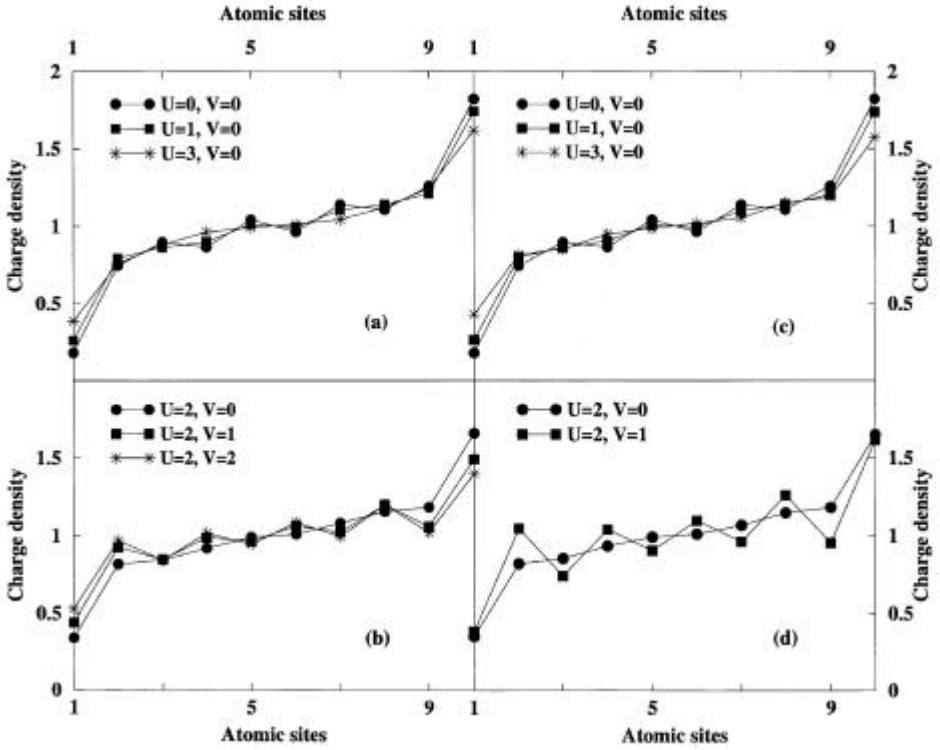

Figure 1. Comparisons of charge densities as a function of atomic sites for various *U* and *V* parameters with mean-field (**a** and **b**), and exact (**c** and **d**).

As mentioned above, earlier calculations of the spatial potential profile were based on Hartree approximation of the molecular Hamiltonian. Our calculations are done in Hartree–Fock basis. Since we have treated the model in a mean-field sense, we compare and contrast the charge densities for a number of Hubbard parameters by diagonalizing the exact model Hamiltonian in its original form, (6), in the exact Fock space basis. Since the Fock space dimension increases exponentially with the number of sites and we need an iterative solution for the convergence of the potential profile, we have chosen a 10 sites molecular chain. In figure 1, we present charge densities for varying Hubbard *U*, and varying *V* parameters for a fixed *U* value. As can be seen, for small to large Hubbard repulsion, and for variation in *V* values, the mean-field charge densities compare fairly well with the exact calculation. There are two spin-orbitals per atomic site next to each other and the mean-field results shown here are for each atomic site, adding contributions from both the spin-orbitals. Since the system is half-filled, at zero bias (not shown here) both the spin-orbitals have the same amount of charges and *z*-component spins (with opposite signs), in every atomic site for any value of *U*. The densities are uniform in the middle of the chain but show alternations near two ends, due to open boundary effects. However at finite bias, although in a given atomic site, the charge densities as well as the absolute values of the spin densities (not shown) are same in two of its spin-orbitals, the overall density pattern becomes different, such that in one end of the chain there is

depletion in charge densities while on the other end there is accumulation of charges. Furthermore, as can be seen, the induced polarisation due to the external field decreases with increase in U. This is quite easy to understand, since, increase in U localises the charges, and so the effective field the system experiences is smaller for larger U values. A similar situation arises when we include V in the system. For a small U value ($U = 2$ in this case), inclusion of V reduces the accumulation of charges at one end. And for large U values ($U = 6$), even though the system is completely localised initially, an inclusion of small V leads to accumulation of charges at the ends. An increase in V reduces this accumulation, just like in the case of small U. These variations in charge densities have important consequences in transport processes in the system, which will be discussed later.

In figure 2, we present the self-consistently derived potential profile for a chain of 20 sites. Since we have a number of free parameters to vary, some typical interesting cases are shown. For a tight-binding molecule ($U = 0$, $V = 0$), the potential has the features which has been described by others.[21,22] Hereafter we call this type of variation in spatial potential as the tight binding potential profile (TBPF). Note that, the tight-binding solutions are plane-waves; electrons are completely delocalised all over the molecule. A finite but small Hubbard repulsion induces weak Mott localisation. The potential in this case ($U = 2$, $V = 0$), differs from the tight-binding solution: the gradients are nonzero in

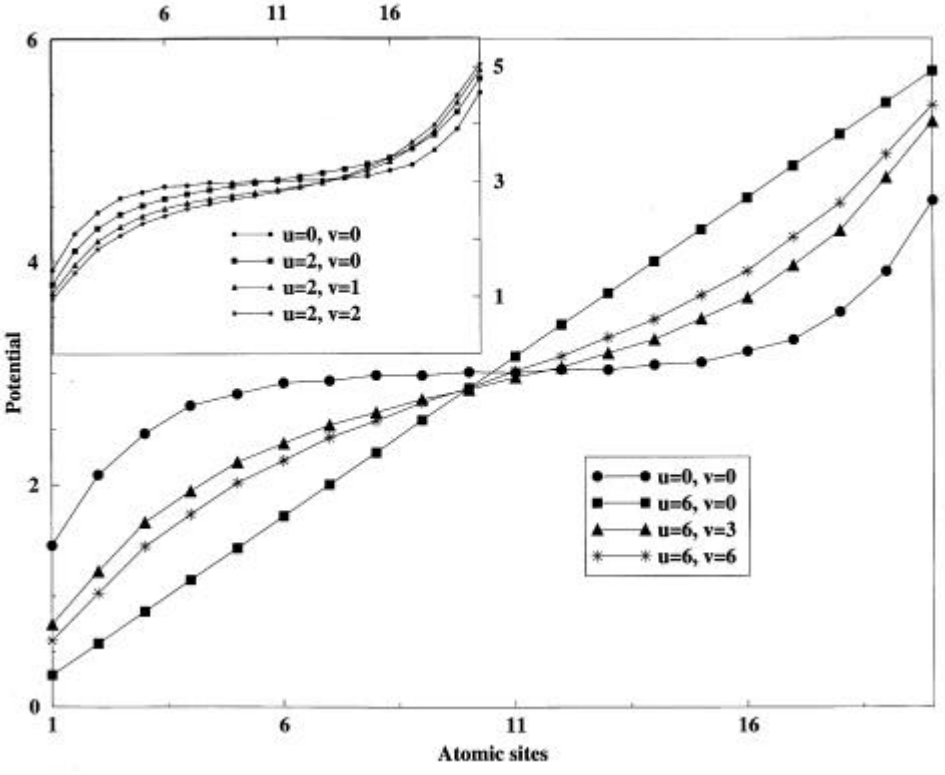

Figure 2. Spatial electrostatic potential profile across the electrode-molecule interface, for various V values in the large U ($U = 6$) limit. Inset shows the same in the small U ($U = 2$) limit.

the middle of the molecule and the potential drop is smaller near the interfaces. For large Hubbard repulsion ($U = 6$, $V = 0$), the profile shows the ramp variation. The general feature is that, increasing the value of U from small ($U = 1$) to large ($U = 6$) takes the potential profile slowly from TBPF to ramp spatial variation. This is quite easy to understand since large U introduces strong site localisation, the electrons are essentially 'particle-like' in the large U limit.

Since the spatial variations of the potential for the small U and large U regions are markedly different, we now try to understand the effects of the extended Hubbard V term in these two regions. For a small U ($U = 2$), increasing the value of V term from 0 to 2, takes the potential profile from TBPF to ramp-like variation. This is apparent in terms of the gradients close to the interface and near the middle of the molecule. And in the large U limit, the potential has a ramp structure without the V term. An increase in V term reduces the gradient near the interfaces and the profile slowly goes from TBPF to ramp-like structure. For an accurate analysis of the potential profile and for comparisons, we have carried out exact diagonalization calculations on small system sizes. We find that the mean-field results compare fairly well with the exact except in the large U, small V limit where the mean field calculations describe the potential profile as TBPF while the exact calculations show a ramp-like profile. An overall picture of the spatial variation of the electrostatic potential for various parameters of the Hamiltonian is summarised in figure 3. Note that in the large U, small V regions (for $U = 5$, 6 and $V = 1$, 2), exact calculations results instead of mean-field have been presented.

To understand the above features in the small and large U limit of the mean field calculations, we should look at the interplay between the band-width due to the kinetic

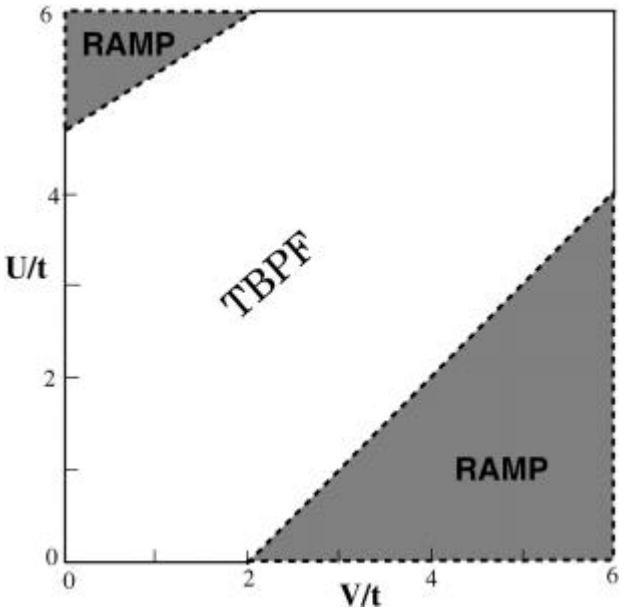

Figure 3. Nature of the potential profile across the wire in the two-dimensional parameters (U and V) space. Results are obtained with mean field calculations, except in the region of large U and small V, where the results from the exact calculations are presented.

energy and the electron interaction effects. As we have discussed before, the V term in this mean-field Hamiltonian essentially renormalizes the hopping strength, thereby increasing the band-width. Since the number of energy levels remain the same, an increase in V essentially produces a wide and sparse band structure. On the other hand, the U term in mean-field limit drives up the molecular energy levels. In the tight-binding model ($U = V = 0$), an increase in the hopping strength results in the potential profile increasingly retaining its initial ramp-like profile. This, as discussed above, is because of the increase in the bandwidth of the energy levels and hence also the HOMO–LUMO gap. This means that a large bias is required to cause a change in the system from its preferred ground state. In the range of voltages applied, the system effectively sees no bias and hence does not undergo much change from the initial ramp-like potential structure. Therefore, for a fixed U, the increase in V tends to produce ramp-like potential in the mean-field, although the exact results show that it actually produces more like TBPF structure. To summarise, both for large U and large hopping extremes, the potential will be ramp-like, however, in the intermediate regime, the feature can vary from TBPF to ramp with a range of different slopes, which is clear from figures 2 and 3.

Next we discuss the consequences of the above discussions on transport properties. Figure 4 represents the current–voltage characteristics of a 20 sites molecular wire with

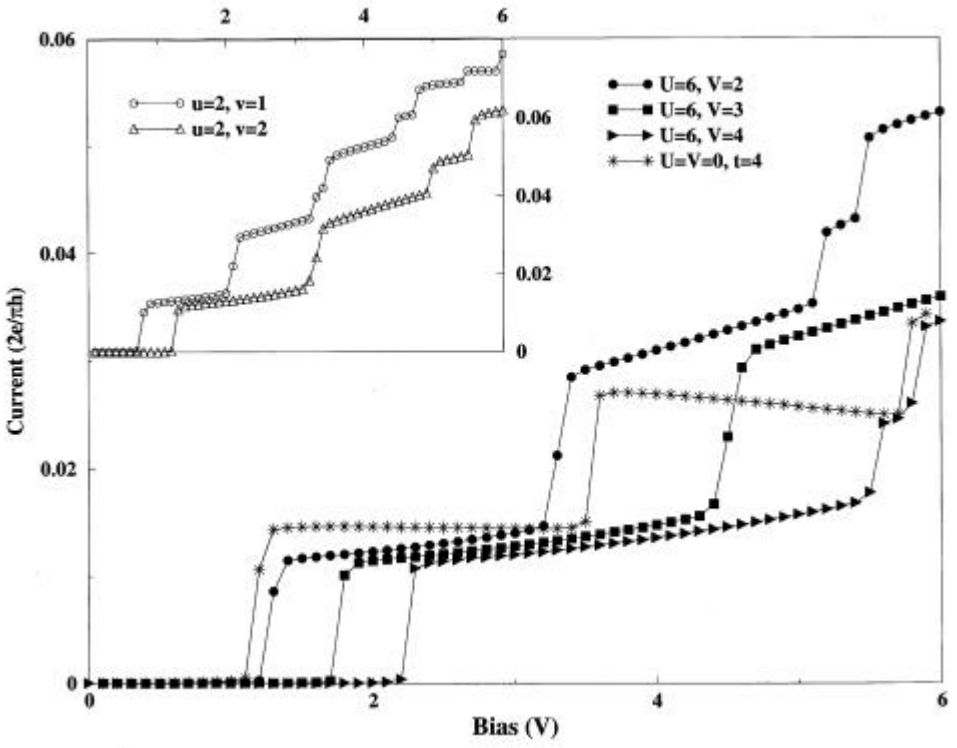

Figure 4. Nonlinear current as a function of applied bias in the large U and small U (inset) limit. The I–V curve for the tight-binding case ($U = V = 0$) with large hopping strength ($t = 4$) is also included to understand the similarity between the t and the V terms.

small and large U values, and the variations of V in each case. The figure shows the unequally spaced jumps characteristic of molecular scale devices, also known as 'molecular resonances' or the 'eigen-value staircase'. The most notable feature from the I–V curves for small U ($U = 2$) and large U ($U = 6$) is that the magnitude of current is quantitatively smaller for larger U values. This, as has been discussed, is due to the increased localisation with increase in U, which reduces the effective field seen by the electrons. In other words, more the localisation, the less is the magnitude of current. We also find that the magnitude of current with ramp potential is always less than the current with the self-consistent field potential. This is true for any values of U and V. And an increasing value of V reduces the current. This again could be because of the increase in the bandwidth and the energy levels which would correspondingly decrease the spectral density, according to (2). Since the spectral density determines the height of the one-electron tunnelling jump and thereby the magnitude of the current, the current in turn reduces for large V.

There are a few other additional features of the I–V curve in figure 4 which are worth mentioning. With increase in V, the number of one-electron tunnelling jumps (within the range of voltages applied) decreases and in between two jumps we find the increase in the width of the voltage plateau. These can be attributed to the fact that the V term renormalizes the hopping strength and consequently increases the total bandwidth of the energy spectrum of the system. Thus the increase in V would mean a larger energy band. However, since the number of one-electron tunnelling levels remain same (system size being the same), the gap between two subsequent energy levels increases. This is to say that the initial bias necessary for switching on the current increases with increase in V value, which is clear from figure 4. We have also included the I–V for the tightbiding ($U = V = 0$, $t = 4$) case in the same figure. This is to show explicitly how the current for an increased value of the hopping integral, compares with the current for larger V values; that the t and V terms behave similarly. The other interesting point is that with electron correlations, we do not find features of Negative Differential Resistance (NDR) which has been earlier observed in the noninteracting models. In the tight-binding model, presence of NDR in I–V curve was attributed to the voltage-induced localisation of the electronic eigen states. In our case, the presence of the spatially varying Hubbard and extended Hubbard terms nullify the effects of voltage induced localisation and in some range of voltages even lead to a Positive Differential Resistance (PDR) in the I–V characteristics.

In summary, we have considered an interacting one-dimensional molecular wire placed between two large metal electrodes. The spatial electrostatic potential profile has been derived solving both Schrödinger and Poisson equations self-consistently. Depending on the parameters of the model, we have shown that the electrostatic potential profile can vary from complete ramp or ramp-like to a function which has large gradient near the chain ends but zero gradient in the middle of the chain. We have shown that the nonlinear current through the molecular wire depend crucially on the potential profile across the wire-electrode interface and the magnitude of the current is less for the ramp potential than for the potential of other form. The importance of electron correlations on nonlinear transport properties of nanoscale devices is shown to be extremely crucial. Efforts are under way to understand the role of structure, electron-correlations and metal-electrode couplings in optimising the nonlinear current in semiconductor nanostructures.

Acknowledgements

This work was supported by the Department of Science and Technology, New Delhi. One of the authors (SKP) expresses deepest gratitude to Prof. C N R Rao, for his continued support and encouragement.

References

1. Jortner J and Ratner M A (eds) 1997 *Molecular electronics* (London: Blackwell)
2. Birge R R (ed.) 1994 *Molecular and biomolecular electronics* (Washington, DC: ACS)
3. Segal D, Nitzan A, Ratner M A and Davis W B 2000 *J. Phys. Chem.* **B104** 2791; Nitzan A *Annu. Rev. Phys. Chem.* (in press)
4. Kergueris C, Bourgoin J P, Palacin S, Esteve D, Urbina C, Magoga M and Joachim C 1999 *Phys. Rev.* **B59** 12505
5. Kergueris C, Bourgoin J P and Palacin S 1999 *Nanotechnology* **10** 8
6. Reed M A, Zhou C, Muller C J, Burgin T P and Tour J M 1997 *Science* **278** 252
7. Tans S J, Devoret M H, Dai H, Thess A, Smalley R E, Geerligs L J and Dekker C 1997 *Nature* (*London*) **474** 474
8. de Picciotto R, Stormer H L, Pfeiffer L N, Baldwin K W and West K W 2001 *Nature* (*London*) **411** 51
9. Datta S 1995 *Electronic transport in mesoscopic systems* (Cambridge: University Press)
10. Aviram A and Ratner M A 1998 *Molecular electronics: Science and technology* (New York: New York Academy of Science) p. 852
11. Samanta M P, Tian W, Datta S, Henderson J I and Kubiak C P 1996 *Phys. Rev.* **B53** R7626
12. Damle P S, Ghosh A W and Datta S 2001 *Phys. Rev.* **B64** 201403
13. Krzeminski C, Delerue C, Allan G, Haguet V and Stievenard D, Frere P, Levillain E and Roncali J 1999 *J. Chem. Phys.* **111** 6643
14. Buttiker M and Landauer R 1982 *Phys. Rev. Lett.* **49** 1739; Buttiker M and Landauer R 1985 *Phys. Scr.* **32** 429
15. Anderson P W 1961 *Phys. Rev.* **124** 41; Newns D M 1969 *Phys. Rev.* **178** 1123
16. Mujica V, Kemp M, Roitberg A E and Ratner M A 1996 *J. Chem. Phys.* **104** 7296
17. Mujica V, Kemp M and Ratner M A 1994 *J. Chem. Phys.* **101** 6849
18. Keiss H G (ed.) 1992 *Conjugated conducting polymers* (Berlin: Springer-Verlag)
19. Pati S K 2003 *J. Chem. Phys.* **118** 6529
20. Tian W, Datta S, Hong S, Reifenberger R, Henderson J I and Kubiak C P 1998 *J. Chem. Phys.* **109** 2874
21. Mujica V, Roitberg A E and Ratner M A 2000 *J. Chem. Phys.* **112** 6834
22. Datta S, Tian W, Hong S, Reifenberger R, Henderson J I and Kubiak C P 1997 *Phys. Rev. Lett.* **79** 2530